

# Meta-Positioning of Carbonitrile Functional Groups Induces Interfacial Edge-On Phase of Oligophenyl Derivatives

Matthias Marschall,<sup>†</sup> Joachim Reichert,<sup>†</sup> Katharina Diller,<sup>†</sup> Svetlana Klyatskaya,<sup>‡</sup> Mario Ruben,<sup>‡,§</sup> Alexei Nefedov,<sup>||</sup> Christof Wöll,<sup>||</sup> Lev N. Kantorovich,<sup>⊥</sup> Florian Klappenberger,<sup>\*,†</sup> and Johannes V. Barth<sup>†</sup>

<sup>†</sup>Physik Department E20, Technische Universität München, 85748 Garching, Germany

<sup>‡</sup>Institut für Nanotechnologie (INT), Karlsruher Institut für Technologie (KIT), 76344 Eggenstein-Leopoldshafen, Germany

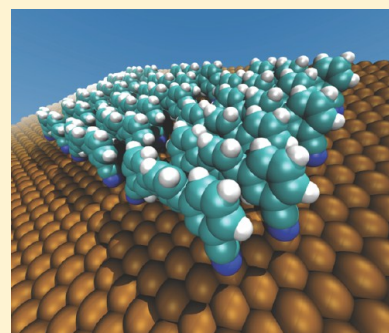
<sup>§</sup>Institute de Physique et Chimie de Matériaux de Strasbourg (IPCMS), CNRS-Université de Strasbourg, 67034 Strasbourg, France

<sup>||</sup>Institut für Funktionelle Grenzflächen (IFG), Karlsruher Institut für Technologie (KIT), 76344 Eggenstein-Leopoldshafen, Germany

<sup>⊥</sup>Department of Physics, King's College London, The Strand, London WC2R 2LS, United Kingdom

## Supporting Information

**ABSTRACT:** We present a combined systematic experimental and theoretical study of the supramolecular organization of a carbonitrile-functionalized oligophenyl on Cu(111) and Ag(111) showing multiple self-assembled structures including a novel edge-on phase at room temperature. We were able to follow the coverage dependent assemblies by means of scanning tunneling microscopy, near-edge X-ray absorption-fine-structure spectroscopy, and X-ray photoelectron spectroscopy and supported the analysis of the experimental results by density functional theory calculations. With increasing coverage the molecular orientation of the building blocks changes from nearly coplanar with the substrate to upright standing. With this reorientation, the stabilizing forces behind the respective bonding motives change from noncovalent molecule–molecule attraction governed by the polar functional groups to metal–organic coordination toward the substrate combined with intermolecular  $\pi$ – $\pi$  interaction.



## INTRODUCTION

Thin molecular films have attracted high interest over the past decade due to their possible application as organic light emitting devices,<sup>1–4</sup> organic semiconductors,<sup>5–7</sup> in photovoltaics,<sup>8</sup> and in nonlinear optics.<sup>9</sup> Two factors are decisively influencing the performance of such devices and are thus required to be controlled: the charge carrier injection from the substrate into the active organic layers and the charge transport within them. For optimizing the transport molecular  $\pi$ -stacking of the involved aromatic systems is an established way to increase the charge mobility.<sup>10–12</sup> For mastering the injection barriers the interaction between the substrate and the constituents of the thin film needs to be understood. Their interplay defines, for example, the charge-transfer properties at the complex interfaces between metals and molecules with strong electron acceptors groups<sup>13–15</sup> or whether the molecular contact layer retains its semiconducting character or adopts more metallic-like features.<sup>16</sup> Not only the choice of the molecular units but also their packing strongly influences the properties of the interface<sup>17</sup> and therefore requires careful control. Different approaches are currently under investigation to steer the packing. For many systems the prevailing molecular superstructure in the first monolayer is defined by the epitaxial influence of the employed substrate.<sup>18–20</sup> With strongly corrugated surfaces a well-defined azimuthal orientation of elongated species can be imposed.<sup>21–23</sup> Moreover, by using adequate growth conditions the template-induced structure of

the interfacial layer can control the arrangement of the full organic thin film.<sup>24–27</sup>

Oligophenyls are an important class of organic building-blocks<sup>28,29</sup> mainly because of their optical properties allowing blue electroluminescence<sup>30</sup> and the emission of polarized light.<sup>31</sup> In thin films, with just a few monolayers of molecular coverage and in the bulk, the organic constituents arrange in a so-called herringbone formation,<sup>29,32–35</sup> i.e., an alternating sequence of different orientations with two molecules making an angle of  $66^\circ$ . There are many hints that for most of the substrates already the interfacial layer is dominated by the according alternating sequence of nearly coplanar adsorbed and strongly tilted  $\pi$ -systems<sup>21,34</sup> referred to as flat-on and edge-on orientations, respectively.

Using carbonitrile-functionalized oligophenyls as tectons generated promising organic<sup>27,36–38</sup> assemblies and metal–organic nanoarchitectures.<sup>39–46</sup> In contrast to the bare oligophenyl building-blocks, recent experiments on Ag(111) showed that terminal carbonitrile (CN) groups in para positions of the rim phenyl rings increase the interaction with the metal substrate leading to a stricter epitaxial order with all molecules adsorbed flat-on even in saturated monolayers, thus suppressing the edge-on adsorption geometries. Starting from

Received: December 3, 2013

Revised: January 13, 2014

Published: January 13, 2014



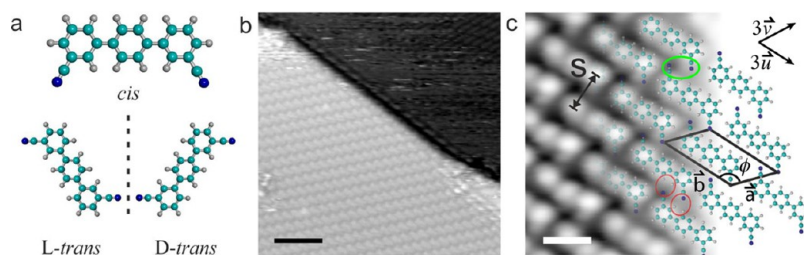


**Figure 1.** Molecular model and STM images of an organic supramolecular network at RT. (a) Atomistic model of the *mNC-pPh<sub>3</sub>-mCN* molecule in *cis* and *trans* conformations. Carbon is shown as cyan, nitrogen as blue, and hydrogen as white spheres. The distance between the two N atoms in the *cis* conformation is 12.56 Å. (b) STM image of a 0.7 ML coverage of *mNC-pPh<sub>3</sub>-mCN* on Cu(111) showing two terraces separated by a monatomic step running from the top left to the bottom right. The higher terrace (bright, lower left part) is filled with the brick network. The lower terrace (darker area, top right part) supports unstable domains (top right corner) surrounded by a 2D molecular fluid. The scale bar represents 50 Å. (c) High-resolution STM image of the brick phase superimposed with the atomistic model, where the interactions are indicated with colored circles (dipolar in green, PARI in red). The surface unit cell vectors  $\vec{u}$  and  $\vec{v}$  are indicated. The brick structure unit cell vectors  $\vec{a}$  and  $\vec{b}$  have a length of 9.3 and 15.0 Å ( $\pm 0.5$  Å), respectively, and form an angle  $\phi$  of  $135^\circ$  between them. The distance  $s$  between the molecular rows is  $6.9 \pm 0.5$  Å. The scale bar represents 9 Å.

such templated monolayers, thin films of all tested species with a backbone length of three to six phenyl moieties inherited this uniform molecular orientation.<sup>27</sup>

Here we investigate the impact of changing the substituents attachment from *para* to *meta* positions on the interfacial packing. We employ the STM+XS approach<sup>47</sup> to study the growth of the prochiral tecton *mNC-pPh<sub>3</sub>-mCN* (Figure 1a) on Cu(111) and Ag(111) with film thicknesses ranging from the submonolayer to the multilayer regime. The measurements have been conducted employing scanning tunneling microscopy (STM), near-edge X-ray absorption-fine-structure (NEXAFS) spectroscopy, and X-ray photoelectron spectroscopy (XPS) and are complemented by density functional theory (DFT) calculations. Our findings reveal the coverage-dependent expression of different self-assembled superstructures whereby the conversion from a known to a previously undiscovered phase involves the reorientation of the building blocks. On the Cu(111) surface regular dense islands prevail in the regime of below 1 monolayer (ML) with the molecules lying flat, i.e., with their  $\pi$ -system plane oriented parallel to the surface. Thereby, a ML is defined as the densest layer covering the complete sample surface with molecules adsorbed in such a flat manner. With increasing coverage, a striking reorientation of the molecular plane lifts off the conjugated  $\pi$ -backbone from the surface and results in a novel edge-on phase with a reduced interaction of the conjugated  $\pi$ -system with the substrate. On the Ag(111) surface a similar reorientation is also found; however, evaporation of small amounts of Co is necessary to induce the change. In connection with the transition in adsorption geometry, a switch of the predominant stabilizing forces takes place. At low coverages, dipolar interaction and proton acceptor ring interaction<sup>48</sup> prevail, while metal-coordinated anchoring combined with  $\pi$ - $\pi$  stacking stabilizes the assembled structures at high coverages. Our main conclusions are supported by DFT calculations of a number of various models for the edge-on phase on the Cu(111) surface.

## EXPERIMENTAL METHODS

**STM Measurements.** All STM measurements were conducted in an ultrahigh vacuum environment working at a base pressure of  $1 \times 10^{-10}$  mbar using a Specs Aarhus type STM. The Cu(111) and Ag(111) single crystal surfaces were cleaned by repeated Ar<sup>(+)</sup> sputtering and subsequent annealing

in order to achieve extended smooth terraces on the surface. The [1,1';4',1'']-terphenyl-3,3''-dicyanide (*mNC-pPh<sub>3</sub>-mCN*, Figure 1a) molecules were evaporated by means of organic molecular beam epitaxy from a quartz crucible held at 440 K while the sample was kept at room temperature (RT). In the case of evaporation of Co atoms on the Ag(111) surface, the samples were exposed to a beam of atoms, produced by heating a Co wire wound around a W filament by driving current through the W wire, subsequent to the deposition of the organic material. The STM measurements were performed at RT.

**Synchrotron Measurements.** The NEXAFS and XPS measurements were performed at the HE-SGM beamline at the BESSY II synchrotron in Berlin. The employed apparatus works at a base pressure in the low  $10^{-10}$  mbar regime and in order to obtain results comparable with the STM measurements the sample preparation have been performed in the same manner. To reduce beam damage especially at high molecular coverage, the sample was held at  $\sim 160$  K during measurements. Multilayer samples were studied with monochromator slit widths of 100  $\mu\text{m}$  resulting in an energy resolution of 0.2 eV for the C K-edge and 0.3 eV for the N K-edge. Spectra of submonolayer and monolayer coverages were recorded with a slit width of 200  $\mu\text{m}$  corresponding to an energy resolution of 0.4 and 0.6 eV for the C and N K-edge, respectively. The data treatment was performed following the procedures described in ref 49.

For the XPS measurements, the excitation energies were 435 and 550 eV for the C 1s and N 1s regions, respectively. The pass energy of the hemispherical analyzer (Scienta R3000) was set to 20 eV for all measurements. Spectra were acquired in normal electron emission geometry. The binding energy scale was calibrated against the Cu 3p<sub>3/2</sub> line of the substrate at 75.1 eV.

## THEORETICAL METHODS

DFT calculations of the molecules on the Cu(111) surface were performed using the plane wave VASP code.<sup>50,51</sup> Electronic exchange and correlation interactions were described using the generalized gradient approximation (GGA) as proposed in ref 52. van der Waals (vdW) interactions were taken into account by applying the Grimme2 correction (DFT-D2)<sup>53</sup> with standard parameters. The calculations were performed using projector augmented-wave pseudopotentials.<sup>54,55</sup> In all calcu-

lations a plane wave cutoff of 500 eV was used, and the  $2 \times 8 \times 1$  Monkhorst-Pack  $k$ -point sampling method<sup>56</sup> with 8 and 2 divisions along the short and long unit cell directions, respectively, was applied. All calculation used a slab model with a  $(7 \times 2)$  unit cell with four atomic layers to represent the Cu(111) surface. This setup corresponds to a rather dense periodic array of the molecules in the edge-on configuration on the surface.

## RESULTS AND DISCUSSION

**STM Measurements of the Low-Coverage Phase.** An atomistic model of the prochiral, ditopic  $mNC$ - $pPh_3$ - $mCN$  is depicted in Figure 1a. It consists of three phenyl rings forming the linear conjugated backbone and a CN group placed in meta position on each of the outer phenyl rings. The  $\sigma$ -bonds between the phenyl rings allow for a rotation of the phenyl rings around the molecular backbone axis. In the gas phase an equal distribution between cis and trans isomers can be assumed.<sup>37,44,57</sup> Upon 2D confinement the rotational degrees of freedom are reduced and three well-defined conformers evolve, namely a cis and two mirror-symmetric trans species (L- and D-trans).

For a coverage of  $\sim 0.7$  ML on Cu(111) the molecules initially assemble in a highly regular supramolecular pattern as depicted in Figure 1b. The image shows two terraces. The brighter upper terrace is covered with a dense-packed molecular layer which can be stably imaged; that is, the absence of streaks indicates that molecules reside on their positions during the time of scanning over them. On the lower terrace (dark area) unstable island borders surrounded by a streaky area indicate a dynamic equilibrium between the solid phase and the molecular surface gas. This equilibrium evidence that at RT single molecules that are not inside a condensed domain are highly mobile on the bare metal surface. In high-resolution STM data (Figure 1c) it becomes evident that a single molecule appears as a rod-like protrusion (bright) consisting of three connected protrusions originating from the phenyl rings. The CN groups produce lateral extensions of the rods which can only be resolved with appropriate tips. In the direction of the long molecular axis the molecules form chains that are stacked side by side with an offset resembling a brick wall, therefore we call this assembly the brick structure. Recent experiments on Ag(111)<sup>37</sup> showed that at low temperature (6 K) the surface fluid is condensed into 1D chains oriented along the high-symmetry directions of the crystal. These molecular chains are constructed from trans molecules in an enantiopure fashion. The same study demonstrated that also the islands consist of homochiral trans isomers and suggested that the intermolecular attraction resulted from the interaction between CN groups and phenyl moieties of the adjacent molecules. These findings suggest the same topology for the atomistic model of the brick structure (Figure 1c) that agrees well with the features of the STM image. It turns out that the size and the shape of the unit cell ( $|\vec{a}| = 9.3 \text{ \AA}$ ,  $|\vec{b}| = 15.0 \text{ \AA}$ ,  $\phi = 135^\circ$ ) is nearly identical to that on Ag(111).<sup>37</sup> Considering the Cu(111) atomic lattice, it is deduced that the measured superstructure is commensurate with the underlying surface with the vector  $\vec{b}$  being oriented along one of the  $\langle \bar{1}10 \rangle$  surface directions and exhibiting a length of six nearest-neighbor distances (amounting to the total length of  $15.34 \text{ \AA}$  assuming a theoretic Cu nearest-neighbor distance of  $2.556 \text{ \AA}$ ) and a vector  $\vec{a}$  being rotated by  $133.9^\circ$  with respect to  $\vec{b}$  and having a length of  $9.22 \text{ \AA}$ . The unit cell of the superstructure is given in matrix notation as

$$\begin{pmatrix} \vec{a} \\ \vec{b} \end{pmatrix} = \begin{pmatrix} 1 & 3 \\ -6 & 0 \end{pmatrix} \begin{pmatrix} \vec{u} \\ \vec{v} \end{pmatrix}$$

where  $\vec{u}$  and  $\vec{v}$  are the primitive vectors of the atomic lattice. As discussed in detail in our earlier work,<sup>37</sup> with the 3-fold symmetry of the substrate and the existence of D- and L-trans enantiopure islands the structure exists in six orientational domains.

Carbonitrile functional groups have been successfully used to steer interfacial self-assembly before.<sup>27,36,38,46,58–61</sup> The related theoretical work<sup>48,60–62</sup> demonstrated that dipolar interaction between neighboring antiparallel-oriented carbonitrile groups as well as the so-called proton acceptor ring interaction<sup>48</sup> (PARI) between a carbonitrile group and a nearby phenyl ring are driving forces behind the attraction between molecules with such functional groups. Assuming that the presence of the surface leads to a minor change of the bonding properties of the CN groups, we expect for the geometry exhibited here that both forces contribute considerably to the formation of the brick structure. The offset between the two axes of antiparallel CN groups (highlighted in green in Figure 1c) amounts to  $\sim 4 \text{ \AA}$ , the distance between a terminal N atom and the neighboring H atoms (highlighted in red in Figure 1c) measures  $\sim 3 \text{ \AA}$ . The similarity to the values for geometries optimized for dipolar interaction ( $3.857 \text{ \AA}$ , ref 62) and for PARI ( $2.9 \text{ \AA}$ , ref 48) strongly support our interpretation.

**Coverage Dependent Structure Formation.** Next we discuss the coverage dependence of the molecular superstructures formed on the Cu(111) surface. After dosing only a small amount of molecules ( $< 0.1$  ML) only the step edges are decorated (see Figure S1). After having filled up all the lower sides of the step edges excess molecules form a surface gas. Such a situation is present on the lower terrace in Figure 1b. For coverages below 1 ML extended regular islands exhibiting the brick structure described above dominate the sample surface. Further increase of the adlayer coverage results in several pronounced changes of the observed organic pattern.

Figure 2a shows an STM image of a sample with a coverage of  $\sim 1.2$  ML. It reveals periodically repeated superstructures consisting of two straight and one zigzag shaped molecular line (highlighted in blue), thus referred to as mixed phase. An analysis of a large number of STM images showed that the zigzag lines are always confined by double rows of linear structures, but regions with consecutive double rows could be found as well. The lines are always following a substrate high-symmetry direction (indicated with the white lines in the lower right corner). The zigzag structure can be explained by planar molecules like in the brick structure which are arranged in a zigzag fashion. The linear lines, however, exhibit a rather short interline spacing  $e = 6 \pm 0.5 \text{ \AA}$ , which is too small for planar molecules. This signals that molecules tilt away from the surface to accommodate into these thin lines.

After increasing the coverage to  $\sim 1.5$  ML, we find that the organic layer exhibits a novel phase (Figure 2b) consisting of broad ribbons (highlighted in blue), rotated with respect to the high-symmetry directions and exhibiting irregular borders. They are interrupted by narrow trenches which appear darker in the image. The ribbons feature an average width of  $l = 50 \pm 1.5 \text{ \AA}$  and contain regularly spaced line segments which are oriented along the high-symmetry directions. In the high-resolution image (see Figure 2c) no substructure can be seen within the molecular lines making it difficult to explore the

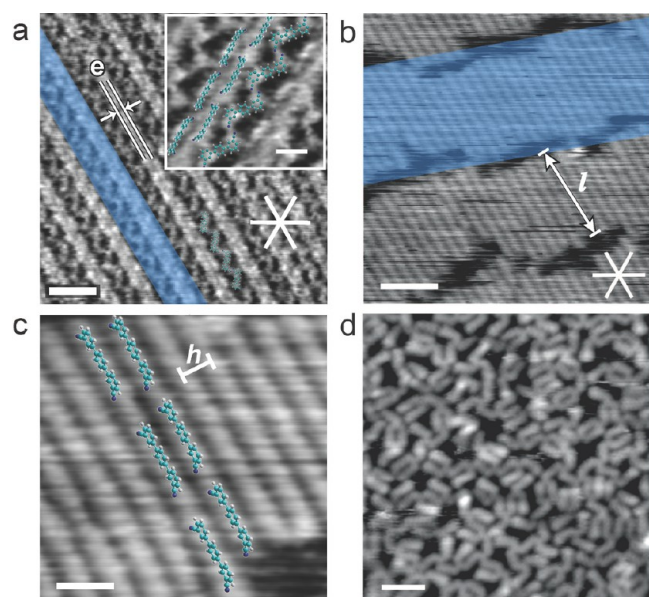


**Figure 2.** Molecular resolution STM images of the coverage dependent assemblies of *mNC-pPh<sub>3</sub>-mCN* on Cu(111) at RT. (a) The mixed phase formed at a coverage of 1.2 ML consists of superstructures (blue) incorporating two linear and one zigzag lines that are oriented along one of the high-symmetry directions of the substrate (white lines) indicated at the bottom right of the image. The interline spacing  $e = 6 \pm 0.5 \text{ \AA}$  of this phase is indicated. The scale bar represents 30  $\text{\AA}$ . The atomistic models of the molecules superimposed to the STM data in the inset (scale bar equals 10  $\text{\AA}$ ) depict the tentative structure of the phase. (b) STM image of the ribbon phase appearing at a coverage of  $\sim 1.5$  ML and featuring stripe structures oriented along the high-symmetry direction of the substrate. The ribbons (blue) exhibit a preferred width of  $l = 50 \pm 1.5 \text{ \AA}$ . The scale bar represents 30  $\text{\AA}$ . (c) High-resolution STM image of the stripes being separated by an interline spacing of  $h = 5.5 \pm 0.5 \text{ \AA}$  superimposed with atomistic models of the molecules visualizing the ribbon width corresponding to approximately three organic units. Since the constituents are mobile, no adsorption site preference can be inferred from the superimposed models. The scale bar represents 10  $\text{\AA}$ . (d) STM image of a random metal–organic coordination network after annealing the sample at 370 K. The scale bar represents 30  $\text{\AA}$ .

assembly in atomistic details. We suggest that within this phase the building-blocks exhibit a mobility significantly higher than in the brick phase not allowing to resolve its topographic

features in greater detail. The interline spacing  $h$  is determined to be  $5.5 \pm 0.5 \text{ \AA}$  and thus is even smaller than the distance  $e$ . Our tentative model is superimposed on top of the experimental molecular pattern (see Figure 2c). The width of the ribbons corresponds roughly to three molecules. Again,  $h$  is too small to assume a coplanar adsorption of the molecular backbone, which would result in a much larger separation (cf. the model of Figure 1c showing the line separation  $s$  that is almost 1.5  $\text{\AA}$  larger than  $h$ ). With the orientation of the phenylene backbone plane being close to perpendicular to the surface, the short spacing  $h$  can be accomplished. Thus, the stripes are tentatively associated with edge-on oriented *cis* isomers with their CN groups pointing toward the sample surface and the phenyl rings lifted away from the substrate. The CN groups are known to have a high affinity toward Cu<sup>63,64</sup> and thus could act as anchoring moieties. Kwon et al. showed for an oxadiazole derivative a similar behavior with an interline spacing of 4.8  $\text{\AA}$ .<sup>65</sup> With the lack of interdigitating CN moieties, our tentative model suggests weaker position-specific intermolecular forces, which could provide an explanation for the higher mobility. Importantly, while systematically increasing the molecular coverage, we did not obtain a sample where exclusively the edge-on phase was present at the entire surface. Rather, we always found coexistence of the mixed and the ribbon phase, as demonstrated by Figure S2.

For comparison, Figure 2d depicts a sample onto which an organic layer with a nominal coverage of 2 ML had been evaporated followed by annealing to 370 K. The binding motifs within the network closely resemble those found in earlier work on random string networks<sup>44</sup> which were constructed from three- and 4-fold planar nodal motifs basing on coordination between Co adatoms and the same organic species as used in this study. Even though here the coverage is slightly higher and no Co is present we suggest that the same metal–organic random structure is present (Figure 2d), but with CN end groups being coordinated by Cu adatoms instead of Co adatoms. Accordingly, all molecules are again adsorbed near-to-flat on the surface similar to the orientation in the brick structure. Consistently, temperature treatment up to  $\sim 400$  K of all samples with less coverage, i.e., starting from the brick or the ribbon structures, resulted in a similar metal-directed assembly.

**Co-Induced Reorientation on Ag(111).** Next, we investigated the influence of the substrate on the formation of the edge-on phase by changing from the Cu(111) to the

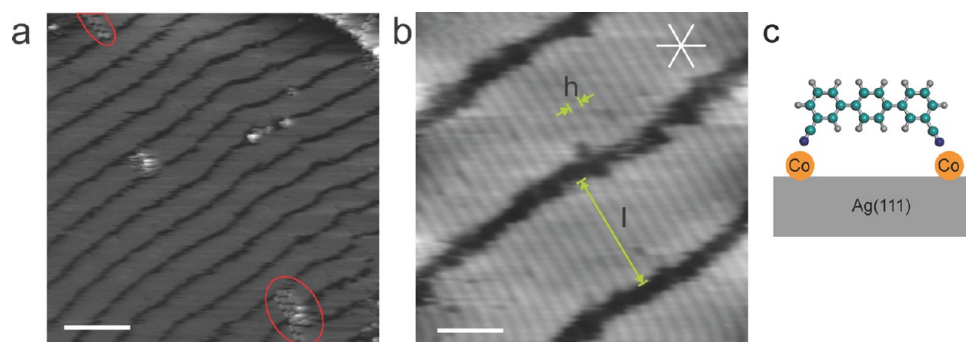


**Figure 3.** Stripe structure on Ag(111) after subsequently evaporating *mNC-pPh<sub>3</sub>-mCN* molecules and Co. (a) Overview image depicting mainly the stripe structure with small areas highlighted (red circles) where the brick structure is still present. The scale bar represents 140  $\text{\AA}$ . (b) High-resolution STM image demonstrating the similar appearance of the pattern as on Cu(111) (cf. Figure 2b). The width of the stripe features  $l$  amounts to 52  $\text{\AA}$  and the interline spacing to about 6  $\text{\AA}$ . Both values are larger than on Cu. The scale bar represents 30  $\text{\AA}$ . (c) Tentative model for the ribbon phase geometry on the Ag(111) surface.

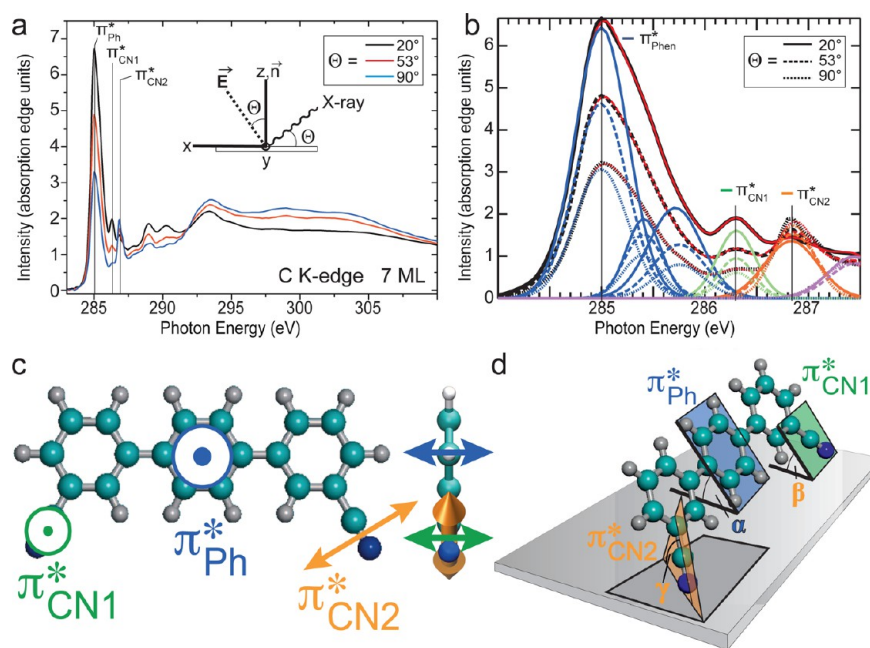


**Figure 4.** Overview on the angle-dependent experimental NEXAFS C K-edge spectra on *mNC-pPh<sub>3</sub>-mCN* and illustration of the probed molecular orbitals. (a) NEXAFS spectra of a *mNC-pPh<sub>3</sub>-mCN* multilayer on Cu(111) and the definition of the X-ray incident angle  $\Theta$ . The evaluated peaks ( $\pi_{\text{Ph}}^*$ ,  $\pi_{\text{CN1}}^*$ , and  $\pi_{\text{CN2}}^*$ ) are marked in the  $\pi^*$  region of the spectra. The inset shows a sketch of the experimental arrangement, where  $\vec{E}$  is the polarization vector of the incident X-ray beam,  $\Theta$  the incident angle, and  $y$  the rotation axis of the experiment. (b) Detail of the  $\pi^*$  region. A fit procedure based on Gaussian functions provides the sum (red) and the intensity of the individual peaks  $\pi_{\text{Ph}}^*$  (blue),  $\pi_{\text{CN1}}^*$  (green),  $\pi_{\text{CN2}}^*$  (orange), and higher resonances (pink). (c) Sketch with top view (left) and side view (right) of the orientation of the orbital  $\pi$  clouds connected to the main resonances used for the investigation of the molecular orientation. For simpler visualization all phenyl rings are displayed in one plane, whereas in reality there is a torsional angle between neighboring rings. (d) Definition of the different angles ( $\alpha$ ,  $\beta$ , and  $\gamma$ ) evaluated from NEXAFS angle-dependence and their relation to the orientations of the different moieties on the surface.

noble-metal Ag(111) surface. For purely organic layers, no assemblies other than the brick phase can be triggered by the increase of molecular coverage. All observed structures are consistent with flat-laying tectons as reported earlier.<sup>37</sup> Since it is known<sup>36,41,43,44</sup> that in the submonolayer regime (coverage  $< 0.4$  ML), Co-directed coordination of the terminal carbonitrile moieties triggers the expression of a variety of nano-architectures, we tested the effect of the presence of Co in the high coverage regime. We found that dosing a small amount of Co atoms on a *mNC-pPh<sub>3</sub>-mCN* layer with 1.3 ML coverage triggered a transition from the brick structure to a ribbon phase (depicted in Figure 3a) which appears very similar to the one found on Cu(111). However, now the length  $l$  is on average equal to  $52 \pm 0.5$  Å and the interline spacing amounts to  $6 \pm 0.5$  Å. The transformation of the molecular pattern took place while continuously scanning the surface with the STM (see SI Figure S3). In view of the similarities we suggest that also on the Ag(111) surface the ribbon phase consists of edge-on oriented organic units. However, the fact that without Co adatoms only the brick pattern is observable even for higher coverages together with the well-established coordination of CN functional groups toward Co atoms via the nitrogen lone-pair<sup>39,41,44,46,59</sup> suggests a coordination motif with Co adatoms between surface and molecules as qualitatively depicted in Figure 3c. This raises the question of whether adatoms are incorporated into the ribbon phase on Cu(111) in a similar manner or not.

**NEXAFS Measurements.** To corroborate and quantify the coverage-dependent molecular reorientation in the organic adlayer, NEXAFS measurements have been performed. Earlier NEXAFS investigations with the *mNC-pPh<sub>3</sub>-mCN* molecule on

Ag(111) indicated a nearly flat adsorption geometry with the  $\pi$ -system almost parallel to the surface for submonolayer<sup>37</sup> and monolayer (see SI Figure S4) coverages. In this “flat” geometry the steric hindrance between the H atoms of adjacent phenyl rings results in a residual tilt of the individual moieties smaller than  $15^\circ$ . For multilayer coverages the overall orientation stays the same, but the tilt increases by a few degrees (see SI Figure S5). As detailed before, on Cu(111) the apparent molecular structure visualized in the STM images of low coverage samples corresponds to the one measured on Ag(111).<sup>37</sup> In order to verify the similarity of the molecular structure on Ag(111) and Cu(111), NEXAFS measurements have been performed also on Cu(111). In addition, the coverage was stepwise increased to investigate possible changes in the molecular orientation in the different patterns that have occurred in the STM measurements.

The C K-edge of a sample with multilayer coverage grown on Cu(111) was measured (Figure 4a) and compared to that of the Ag(111) multilayer sample (Figure S5). The growth mode on the latter substrate was intensely investigated<sup>27,37</sup> and demonstrated the absence of dewetting. Accordingly, the Ag(111) multilayer spectra are free from the substrate influence and represent a reasonable reference. The similarity of the shape of the spectra obtained for both supports also qualifies the Cu(111) multilayer to be a valid reference of the intact molecule and its electronic structure. The layer thickness was approximately 7 ML as evaluated from the absolute absorption edge signal height. Figure 4a presents the multilayer NEXAFS spectra measured for three different incident angles  $\Theta$  ( $20^\circ$  in black,  $53^\circ$  in red and  $90^\circ$  in blue) where  $\Theta$  is defined as the angle between the  $\vec{E}$ -vector of the X-ray beam and the sample

surface normal  $\vec{n}$  (see inset in Figure 4a). In the  $\pi^*$  region the spectra show three distinct peaks at 284.9, 286.2, and 286.7 eV named  $\pi_{\text{Ph}}^*$ ,  $\pi_{\text{CN1}}^*$ , and  $\pi_{\text{CN2}}^*$  (see Figure 4b). The sharp resonance  $\pi_{\text{Ph}}^*$  and the features at 288.7 and 290 eV can be found at similar energies in benzene and oligophenyl.<sup>34,66–68</sup> The features  $\pi_{\text{CN1}}^*$  and  $\pi_{\text{CN2}}^*$  are not present in the spectra of such species; thus, we assign them to the two perpendicular  $\pi$ -systems provided by the CN groups schematically drawn in Figure 4c. Consistently, recent work<sup>27</sup> showed similar resonances for *p*NC-*p*Ph<sub>3</sub>-*p*CN oligophenyl derivatives featuring the CN moieties in para positions. Note that the orbitals connected with  $\pi_{\text{Ph}}^*$  and  $\pi_{\text{CN1}}^*$  are aligned in the same direction, namely perpendicular to the molecular backbone plane, whereas  $\pi_{\text{CN2}}^*$  is aligned within the molecular backbone plane, thus perpendicular to the former two, and includes an angle of 60° with the long molecular axis.

For the analysis of the orientation of the different moieties with respect to the surface, we concentrate on the  $\pi^*$  region and use a set of angles ( $\alpha$ ,  $\beta$ , and  $\gamma$ ; explained in Figure 4d) to characterize the molecular geometry. Fortunately, the angles resolved from the NEXAFS analysis can be directly linked to this description. The angles  $\alpha$  and  $\beta$  represent the tilt angles of the direction of the  $\pi$  systems ( $\pi_{\text{Ph}}^*$ ,  $\pi_{\text{CN1}}^*$ ) with respect to the surface normal  $\vec{n}$ , whereby the  $\pi_{\text{CN1}}^*$  orbital is oriented perpendicular to the adjacent phenyl ring. In contrast, the direction of the orbital assigned to resonance  $\pi_{\text{CN2}}^*$  (orange) is oriented within the plane of the adjacent phenyl ring and perpendicular to the long axis of the CN group. The angle  $\gamma$  is defined between this direction and  $\vec{n}$ . If a molecule is adsorbed flat with its molecular backbone plane parallel to the surface, the angles  $\alpha$  and  $\beta$  would be 0° and  $\gamma$  would be 90°, respectively. In contrast, if a molecule is adsorbed with its molecular backbone perpendicular to the surface, the angles  $\alpha$  and  $\beta$  would be 90°, but the angle  $\gamma$  would be 60°. The limited range of values that  $\gamma$  can adopt results from the fact that the CN groups are connected to the phenyl rings in meta position and thus point away from the long molecular axis of the backbone. Further confirmation for our interpretation of the resonances are provided through calculations by Rangan et al.<sup>69</sup> and Piantek et al.<sup>70</sup> employing benzonitrile and dimetacyano azobenzene, respectively.

An example of the analysis of the  $\pi^*$  region is depicted in Figure 4b. Each of the three resonances was fitted with up to three Gaussian functions in the  $\Theta = 20^\circ$  spectrum. The relative energy and peak width were kept constant for all of the spectra. The fitted peak shapes for  $\pi_{\text{Ph}}^*$ ,  $\pi_{\text{CN1}}^*$ , and  $\pi_{\text{CN2}}^*$  are shown in blue, green and orange, respectively. The larger width of the peak  $\pi_{\text{Ph}}^*$  compared to the other resonances can be explained by the excitation of different C 1s initial states of the different carbon atoms of the phenyl rings into the same unoccupied state while for the CN related peaks only one initial state is relevant.<sup>27,71</sup> The variation of the incident angle causes changes in the peak intensity which can be evaluated from the fit. From this angle dependence the three angles ( $\alpha$ ,  $\beta$ , and  $\gamma$ ) presented in Figure 4d can be calculated.

In the NEXAFS spectra displayed in Figure 4b the peaks  $\pi_{\text{Ph}}^*$  and  $\pi_{\text{CN1}}^*$  decrease with increasing  $\Theta$  while the peak  $\pi_{\text{CN2}}^*$  increases. The analogous behavior of the two former peaks is expected, since the orbitals are coplanar (see Figure 4c,d). The opposite variation of the intensity of peak  $\pi_{\text{CN2}}^*$  is thus consistent with the different orbital symmetry. An analysis of the  $\Theta$  dependences according to ref 72 results in  $\alpha = 40^\circ \pm 5^\circ$ ,  $\beta = 35^\circ \pm 5^\circ$ , and  $\gamma = 65^\circ \pm 5^\circ$ . Consequently, the orientation

of the molecular backbone and the CN-groups deviate strongly from the surface plane, in contrast to the multilayer epitaxy of the para-substituted species.<sup>27</sup>

Next we compare 0.7 and 1.5 ML films where in the STM measurements the brick and the ribbon structures prevailed, respectively. In Figure 5a the NEXAFS C K-edge spectra for a

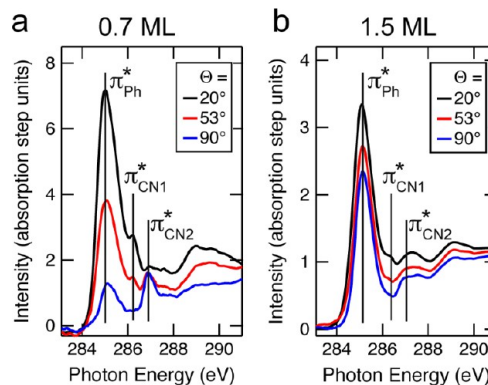


**Figure 5.** Angle-dependent high-resolution NEXAFS C K-edge spectra of *m*NC-*p*Ph<sub>3</sub>-*m*CN on Cu(111) for coverages at which the brick (a) and the striped ribbon structure (b) prevail. (a) NEXAFS spectra of the  $\pi^*$  region of a sample with 0.7 ML molecular coverage. The pronounced dichroism indicates nearly planar adsorbed molecules. (b) NEXAFS spectra of the  $\pi^*$  region of a sample with a coverage of  $\sim 1.5$  ML. The dichroism is strongly reduced compared to (a) and confirms the reorientation of the molecules resulting in a strongly tilted molecular plane.

molecular coverage of 0.7 ML are depicted. The same three  $\pi^*$ -resonances as in the multilayer clearly appear again, but with an increased line width. The broadening of the resonances is a combined effect of the reduced resolution due to the larger slit widths and the faster decay of the core hole due to the presence of the metal substrate. The dichroism is stronger than for the multilayer case. The angles obtained from the analysis of the  $\Theta$ -dependent peak intensities are  $\alpha = 20^\circ \pm 5^\circ$ ,  $\beta = 25^\circ \pm 5^\circ$ , and  $\gamma = 70^\circ \pm 5^\circ$ . The molecules in the submonolayer are hence oriented nearer to planar to the surface than in the multilayer. The NEXAFS analysis clearly confirms the near-to coplanar adsorption in the brick structure as suggested by the STM measurements on Cu(111) (cf. Figure 1). The deviation from the perfectly planar orientation is more than the experimental error; it is also more pronounced than for the same molecule on Ag(111).<sup>37</sup> We suggest that on Cu(111) the N terminations of the functional groups are pointing slightly more toward the substrate than on the Ag(111) surface, however consistently with the STM-analysis, apart from that the overall adsorption geometry seems to be similar to the one found on Ag(111).<sup>37</sup>

The NEXAFS C K-edge spectra presented in Figure 5b were recorded for a molecular coverage of approximately 1.5 ML grown at RT. Again the shape of the spectra is dominated by the  $\pi_{\text{Ph}}^*$  resonance from the molecular phenyl backbone. In comparison with the previous 0.7 ML coverage distinct changes can be found. The maximum intensities of  $\pi_{\text{CN1}}^*$  and  $\pi_{\text{CN2}}^*$  are reduced and the dichroism is clearly smaller. The changes in the NEXAFS spectra become most prominent after the analysis of the normalized peak intensities. The previously small angles for  $\alpha$  and  $\beta$  (in the submonolayer) are markedly raised to  $\alpha = \beta = 45^\circ \pm 5^\circ$ . Consistently, the angle indicating  $\pi_{\text{CN2}}^*$  is slightly reduced to  $\gamma = 60^\circ \pm 5^\circ$ . These changes indicate that the molecular backbone tilts with respect to the surface with

increasing coverage and support the structural changes deduced from the STM analysis.

In order to complement the NEXAFS C K-edge data, spectra at the N K-edge have been recorded (see Figure 6a–c). All

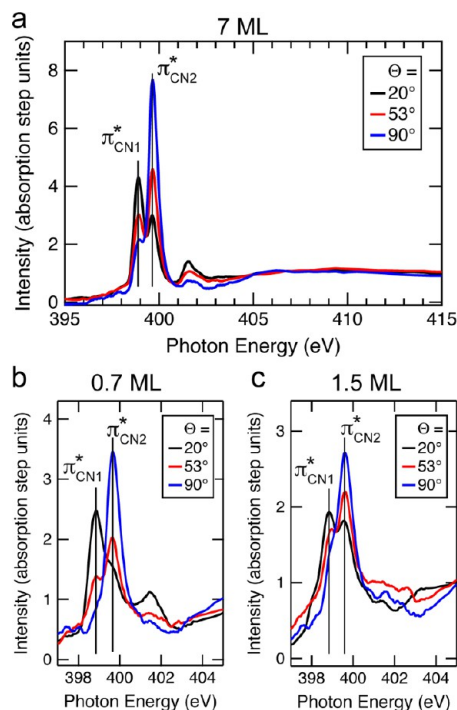


**Figure 6.** Angle-dependent NEXAFS N K-edge spectra at 20°, 53°, and 90° of the photon incident angle  $\Theta$  on Cu(111) with different molecular coverage of *mNC-pPh<sub>3</sub>-mCN* at 160 K.  $\pi_{\text{CN1}}^*$  and  $\pi_{\text{CN2}}^*$  are the prominent features resulting from the carbonitrile group. (a) Spectra from a multilayer sample with  $\sim 7$  ML molecular coverage. (b) Spectra for 0.7 ML molecular coverage. (c) Spectra for a molecular coverage of 1.5 ML.

outlined data were acquired from the same samples as the corresponding carbon spectra. In Figure 6a the spectra of a multilayer with  $\sim 7$  ML coverage are presented. Two  $\pi^*$  resonances at 399.3 and 400.1 eV are the prominent features. They originate from the two  $\pi^*$  orbitals of the CN group ( $\pi_{\text{CN1}}^*$  and  $\pi_{\text{CN2}}^*$ ) as mentioned above (see Figure 4c,d) and discussed in refs 27 and 73. These orbitals are oriented perpendicular to each other as shown in Figure 4c,d. In the range of 401–403 eV another resonance is visible in the multilayer (see Figure 6a) which corresponds to a  $\pi^*$  resonance oriented parallel to the  $\pi_{\text{CN2}}^*$  plane.<sup>69</sup> The positions and angle-dependencies of the resonances  $\pi_{\text{CN1}}^*$  and  $\pi_{\text{CN2}}^*$  agree with DFT calculations of Carniato et al. in the gas phase<sup>73</sup> and results by Rangan et al. on Si(001).<sup>69</sup> The analysis of the molecular adsorption geometry is focused on the first two resonances, which exhibit a strong dichroism. The data analysis of the resonance intensity for the multilayer preparation reveals an angle  $\beta = 35^\circ \pm 5^\circ$  and  $\gamma = 65^\circ \pm 5^\circ$  for the  $\pi_{\text{CN1}}^*$  and  $\pi_{\text{CN2}}^*$  plane with respect to the sample surface. This is in good agreement with the data obtained from our analysis of the C K-edge in Figure 4a presented above.

Figure 6b presents NEXAFS N K-edge spectra of the submonolayer regime (0.7 ML). The shape of the resonance distribution is comparable to the multilayer, but the differences of the intensities are stronger. For example at  $\Theta = 90^\circ$  the  $\pi_{\text{CN1}}^*$  resonance almost vanishes, while at  $\Theta = 20^\circ$  the  $\pi_{\text{CN2}}^*$  resonance

is reduced to a shoulder. This suggests an orientation of the  $\pi_{\text{CN1}}^*$  plane almost coplanar to the metal surface. The quantitative analysis of the resonances revealed an angle  $\beta$  of  $25^\circ \pm 5^\circ$  and  $\gamma$  of  $70^\circ \pm 5^\circ$  and supports the suggested model of the coplanar adsorption of the molecules.

After having increased the coverage to  $\sim 1.5$  ML the resonance intensities are considerably changed as depicted in Figure 6c. The analysis of the  $\Theta$ -dependences of the peaks reveals an angle  $\beta = 45^\circ \pm 5^\circ$  and  $\gamma = 60^\circ \pm 5^\circ$  indicating a tilt of the molecular backbone plane away from the sample surface in accordance with the analysis of the C K-edge presented above (cf. Figure 5b).

An overview of all of the angles evaluated from the NEXAFS data is given in Table 1. The data of both edges are consistent.

**Table 1.** Overview of the Angles Defining the Orientation of the Molecular Moieties with Respect to the Surface As Determined by the Analysis of the NEXAFS C and N K-Edge Spectra<sup>a</sup>

		0.7 ML	1.5 ML	7 ML
C K-edge	$\alpha$	20	45	40
	$\beta$	25	45	35
	$\gamma$	70	60	65
N K-edge	$\beta$	25	45	35
	$\gamma$	70	60	65

<sup>a</sup>Experimental error is  $\pm 5^\circ$ .

The molecular adsorption geometry is near to flat for a coverage of 0.7 ML and the phenyl backbone is strongly tilted with respect to the surface for 1.5 ML.

**XPS Measurements.** Along with the NEXAFS spectra, XPS data have been acquired for the N 1s and C 1s regions. Figure 7a presents an overview of the subsequent XP spectra at the N 1s region with increasing coverage ranging from 0.7 ML to  $\sim 7$  ML. For the first preparation with 0.7 ML (see Figure 7a, the lower curves) one peak (blue) is prominent at 399.5 eV ( $N_a$ ) which we assign to the N atoms of the molecules in the brick structure. Recent XPS measurements by Piantek of azobenzene derivatives on Cu(001) exhibited a peak at 399.6 eV that was interpreted to originate from a physisorbed species.<sup>70</sup> Rangan et al. found a peak at 399.5 eV for benzonitrile on Si(001).<sup>69</sup> Following their interpretations we suggest that in the brick structure the N atoms exhibit a physisorbed state where the N lone pair is mainly interacting with the neighboring molecules, rather than with the Cu substrate. Such a bonding type is consistent with the lateral positioning suggested by STM and the mostly planar adsorption geometry indicated by NEXAFS.

A tiny side peak ( $N_b$ , green) is also visible, which is attributed to the adsorption of the molecules at step edges such that the carbonitrile groups coordinate to the step atoms (see Figure S1). By increasing the molecular coverage the area of the peak with a binding energy of  $\sim 398.4$  eV, designated as  $N_b$ , increases continuously until 1.5 ML. Since already at a 0.7 ML coverage all step edges are occupied, the increase of peak  $N_b$  must be related to one or several different chemical species. In order to determine further possible origins of this signal, an annealing experiment with the maximum temperature of up to 400 K (Figure 7b) was conducted based on a preparation of a sample with 0.7 ML coverage. By annealing the sample, the number of Cu surface adatoms is increased.<sup>74,75</sup> STM measurements (see Figure 2d) suggest, consistently with earlier results,<sup>44</sup> that in

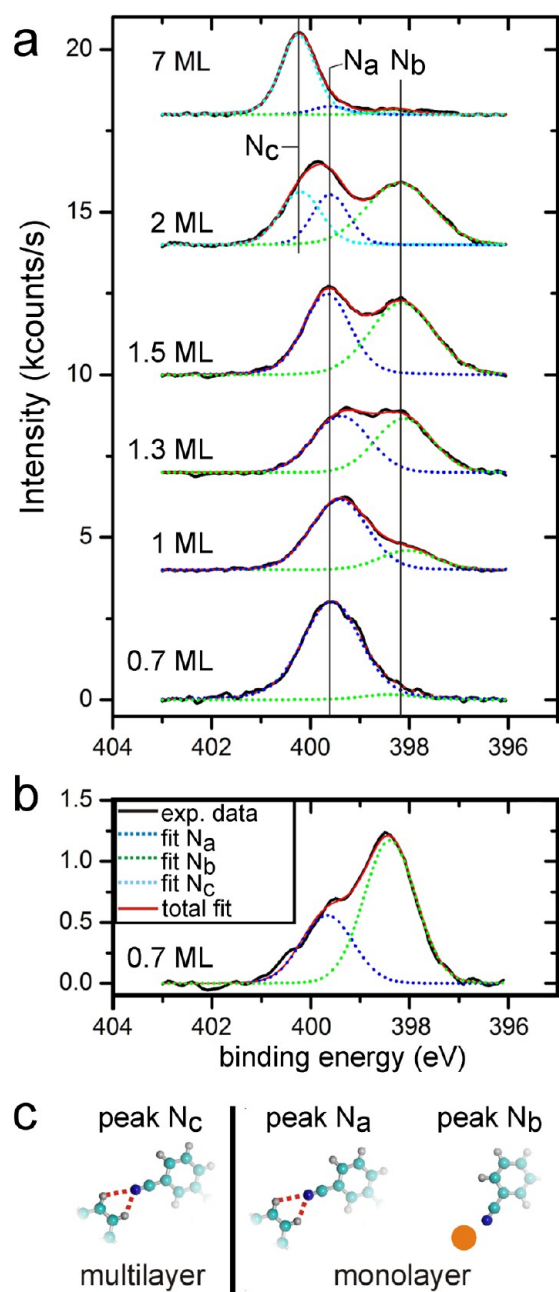


**Figure 7.** XP spectra of *mNC-pPh<sub>3</sub>-mCN* on Cu(111) with increasing molecular coverage taken at 160 K. (a) N1s XP spectra with molecular coverage increasing from 0.7 to 7 ML. (b) XP spectra of the N 1s region of a sample with a molecular coverage of 0.7 ML after annealing to 400 K. Same ordinate scale as in panel a. (c) The atomistic models display the interaction schemes in the vicinity of the surface (monolayer) and embedded in the purely organic film (multilayer) leading to the different peak positions ( $N_a$ ,  $N_b$ , and  $N_c$ ).

such samples the dicyanide molecules remain nearly flat on the surface and coordinate to Cu adatoms forming three- and 4-fold motives in a porous 2D metal–organic network. The annealing experiment demonstrates that differently coordinated CN ligands generate XPS signal intensity at binding energies so similar that they can not be distinguished with our setup. For these reasons we assign the peak  $N_b$  to Cu coordinated N species; however, we assume that during the series of samples different types of Cu coordinated N atoms evoke the seemingly identical signal. It is worth mentioning that in principle there

should be a spectroscopic difference between a CN group of a planar molecule coordinated to a Cu adatom and one of an edge-on molecule coordinated to Cu atoms of the surface. Unfortunately, the physical width of the peaks together with the limited experimental resolution prevent a conclusive distinction. The binding energy of peak  $N_b$  is consistent with earlier reports showing that metal-coordinated CN is characterized by binding energies in the vicinity of 398.5 eV.<sup>15,76</sup>

At 2 ML coverage, a third peak  $N_c$  at 400.2 eV (light blue) arises. In the multilayer system a peak at the same energy dominates the spectra, and we therefore assign it to the nitrogen in the CN functional group connected to molecules not in contact with the surface.

Atomistic models in Figure 7c illustrate our understanding of the local environment of the N atoms resulting in the different peak positions of the related XPS signals. The systematic growth of the  $N_b$  peak with increasing coverage is consistent with the STM and NEXAFS data discussed above. For low coverage, where only the brick structure is present, the  $N_b$  peak intensity is negligible. With increasing coverage an increasing portion of the molecules are forced into the edge-on configuration, i.e., they reorient and coordinate with the CN groups to the surface. Thus, the XPS series agrees with the appearance of the ribbon phase at higher coverages. Furthermore, the XPS data indicate the impossibility to obtain a sample with only edge-on oriented molecules. Consistently, the coexistence of brick and edge-on phases was also observed with the STM for appropriate coverages (cf. Figure S2).

**DFT Modeling.** For a better understanding of the ribbon phase featuring edge-on oriented molecules, we performed DFT-D2 calculations of various systems with linkers in the *cis*-conformation on a four-layer slab of Cu atoms with and without Cu adatoms coordinating the CN group. To be able to compare the stabilities of these systems, which have different numbers of Cu atoms, we calculated the Gibbs free energy  $G$  assuming that the surface system is in thermodynamic equilibrium with the gas of the molecules, where

$$G = E_{S+M} - \mu_{Cu}N_{Cu} - \mu_{mol}$$

Here  $E_{S+M}$  is the DFT energy of the combined surface and molecule system,  $\mu_{Cu}$  the chemical potential of a Cu atom taken from the Cu bulk calculation, and  $\mu_{mol}$  the chemical potential of the molecule taken from the DFT energy of the molecule in the gas phase. The system with the lowest  $G = 17.36$  eV is depicted in detail in Figure 8. It combines bidentate coordinated, upright standing molecules with no Cu adatoms present (Figure 8a). The unit cell is assumed to be commensurate and its vectors have the length of seven and two nearest neighbor distances (17.9 and 5.1 Å), respectively, with the angle of 60° between them (Figure 8b). The side view (Figure 8c) of the system demonstrates the orientation angles of the phenyl rings. The terminal phenyl moieties to which the CN functional groups are linked are tilted by 59° and 42° away from the substrate, while the central phenyl ring exhibits an angle of 80° with the surface.

An overview of all systems is given in Figure S7 along with a discussion of the energetics of the different configurations. From this discussion it becomes clear that the structures with coordination to surface atoms (Figure S7A,D) are energetically preferred by ~0.6–1 eV over geometries incorporating adatoms (Figure S7B,C,E). Thus, from theory point of view there is no need to involve Cu adatoms in order to explain the formation of the edge-on phase on Cu(111) in contrast to the

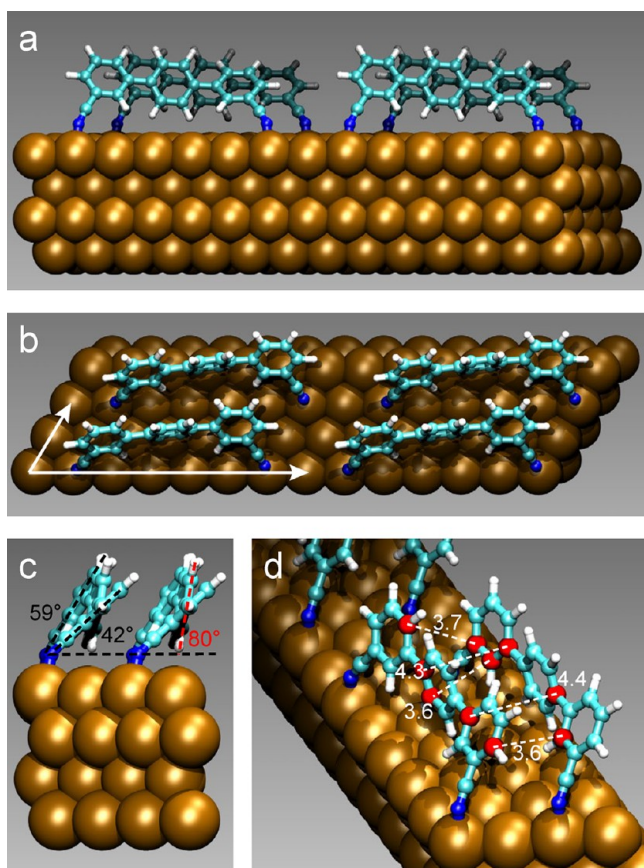


**Figure 8.** DFT-D2-optimized geometry of the system with the lowest free energy  $G = 17.36$  eV. (a) Front view showing the coordination interactions between the N atoms and the surface. (b) Top view visualizing the unit cell vectors (white). (c) Side view giving the orientation angles of the outer (black) and the inner (red) phenyl rings with respect to coplanarity to the surface. (d) Selected distances between highlighted atoms (red) for estimating an average  $\pi$ -stacking distance.

requirement of Co adatoms on Ag(111). From other experiments, it is known<sup>77–82</sup> that on the Cu(111) surface annealing temperatures well above 300 K are necessary for the formation of self-assembled structures which rely on the presence of adatoms, while at RT no such architectures evolve. Therefore, we suggest that the edge-on phase consists mainly of molecules in a configuration similar to the one depicted in Figure 8. However our results also signal that, if free Cu atoms were available, the networks would partially incorporate some of them in a transient fashion.

In the following we compare the experimental findings with the values resulting from this model for the edge-on phase. The theoretical NEXAFS value  $\alpha_{\text{theo}}$  expected for the geometry indicated by DFT can be calculated by averaging the theoretical curves for 59°, 42°, and 80° as described in the SI (cf. Figure S6). The evaluated value amounts to 58°. From the XPS findings we can assume that for the 1.5 ML sample approximately half of the molecules are in the brick structure ( $\sim 20^\circ$ ) and half are in edge-on geometry. Calculating again the NEXAFS expectation angle for such a mixed sample as described yields an angle  $\alpha_{\text{theo,aver}} = 40^\circ$ , which is similar to the experimentally observed  $\alpha = 45^\circ$ . Thus the NEXAFS data can be reconciled with the theoretical geometry of the pure edge-on phase. We point out here that at the temperature of

the NEXAFS measurements, the molecules vibrate and diffuse. Therefore most of the time they will not adopt the structure with the lowest energy, but move between entropically favorable ones. Thus, thermal excitation produces on average more upstanding geometries leading to an even better agreement between theory and experiment. Figure 8d highlights several exemplary distances between carbon atoms (marked red) of adjacent molecules. The average of these distances amounts to 3.92 Å and gives an approximate value for the overall offset between the  $\pi$ -systems. This effective distance is smaller than the separation of the parallel molecular axes (4.427 Å) due to the tilting of the molecules being less than 90°. At such distances  $\pi$ - $\pi$  interactions certainly contribute to the stabilization of the structure.<sup>83</sup> From the STM findings the interline spacing  $h$  was determined to be  $5.5 \pm 0.5$  Å (cf. Figure 2c). This value is significantly larger than the 4.427 Å following from the models assumed in the DFT calculations. For explaining this discrepancy the high mobility of the molecules in the edge-on phase needs to be considered. Theory indicates that N atoms prefer top positions but also only a minor difference between neighboring on top positions, i.e., for going from system B to system D (cf. Figure S7) or changing from displacement vector  $\vec{a}_2$  to  $\vec{a}_1$  in Figure S9. Even though we do not have calculations done for larger unit cells, it is likely that also coordination to atoms of the next row is possible at room temperature. Thus, we tentatively suggest that the measured interline spacing is a result of the dynamic behavior of the molecules in the edge-on phase hopping between favorable on top positions. As sketched in Figure S9, averaging the three smallest possibilities of the unit cell vector  $\vec{a}$  leads to an effective length of 5.3 Å for the unit cell. The corresponding interline spacing (5.17 Å) agrees well with the experimental finding.

Another possibility which might also explain the larger observed value of the interline spacing  $h$  may be a superstructure incommensurate with the underlying lattice or with a larger unit cell. In order to prove or rule out this possibility, much more expensive calculations containing many molecules in the unit cell are required which would go much beyond the scope of our present study.

## CONCLUSION

In conclusion, we have investigated the coverage-dependent assembly of a *para*-oligophenyl species functionalized with terminal CN moieties in meta positions on close-packed coinage metal surfaces. At low coverage the self-assembled domains are stabilized by the combination of dipolar interaction of the functional groups with the proton acceptor ring interaction and consist of molecules adsorbed nearly coplanar to the substrate. In contrast, at high coverage a dynamic ribbon phase prevails featuring “edge-on” oriented organic units having their  $\pi$ -system lifted off from the substrate but remaining anchored by coordination bonding of the CN terminations to the substrate with additional  $\pi$ - $\pi$ -stacking between the molecular backbones. The comparison with earlier work on *para*-substituted species shows that this novel edge-on phase depends on the positioning of the functional groups and does only appear for meta-substituted oligophenyl derivatives. Our findings demonstrate how by careful design of the constituents geometry not only the resulting superstructure but also the interaction and coupling of the different moieties with the substrate can be controlled.

## ■ ASSOCIATED CONTENT

## S Supporting Information

Additional STM images, NEXAFS measurements, an XPS table, and visualizations of the DFT-calculated systems (with and without vdW corrections). This material is available free of charge via the Internet at <http://pubs.acs.org>.

## ■ AUTHOR INFORMATION

## Corresponding Author

\*E-mail: [florian.klappenberger@tum.de](mailto:florian.klappenberger@tum.de).

## Notes

The authors declare no competing financial interest.

## ■ ACKNOWLEDGMENTS

Funding by the European Union via ERC Advanced Grant MolArt (No. 247299) is gratefully acknowledged. A.N. and C.W. acknowledge funding from the "Science and Technology of Nanosystems" Programme (Project No. 431103-Molecular Building Blocks/Supramolecular Networks). The authors acknowledge the Helmholtz-Zentrum Berlin/BESSY II for provision of synchrotron radiation at beamline HE-SGM. Traveling costs for the BESSY measurements covered by Helmholtz-Zentrum Berlin are gratefully acknowledged.

## ■ REFERENCES

- (1) Tang, C. W.; Vanslyke, S. A. Organic Electroluminescent Diodes. *Appl. Phys. Lett.* **1987**, *51*, 913–915.
- (2) Burroughes, J. H.; Bradley, D. D. C.; Brown, A. R.; Marks, R. N.; Mackay, K.; Friend, R. H.; Burns, P. L.; Holmes, A. B. Light-Emitting Diodes Based on Conjugated Polymers. *Nature* **1990**, *347*, 539–541.
- (3) Blochwitz, J.; Pfeiffer, M.; Fritz, T.; Leo, K. Low Voltage Organic Light Emitting Diodes Featuring Doped Phthalocyanine as Hole Transport Material. *Appl. Phys. Lett.* **1998**, *73*, 729–731.
- (4) Sheraw, C. D.; Zhou, L.; Huang, J. R.; Gundlach, D. J.; Jackson, T. N.; Kane, M. G.; Hill, I. G.; Hammond, M. S.; Campi, J.; Greening, B. K.; et al. Organic Thin-Film Transistor-Driven Polymer-Dispersed Liquid Crystal Displays on Flexible Polymeric Substrates. *Appl. Phys. Lett.* **2002**, *80*, 1088–1090.
- (5) Garnier, F.; Yassar, A.; Hajlaoui, R.; Horowitz, G.; Deloffre, F.; Servet, B.; Ries, S.; Alnot, P. Molecular Engineering of Organic Semiconductors - Design of Self-Assembly Properties in Conjugated Thiophene Oligomers. *J. Am. Chem. Soc.* **1993**, *115*, 8716–8721.
- (6) Brown, A. R.; Jarrett, C. P.; de Leeuw, D. M.; Matters, M. Field-effect Transistors made from Solution-Processed Organic Semiconductors. *Synth. Met.* **1997**, *88*, 37–55.
- (7) Chua, L. L.; Zauenseil, J.; Chang, J. F.; Ou, E. C. W.; Ho, P. K. H.; Sirringhaus, H.; Friend, R. H. General Observation of n-Type Field-Effect Behaviour in Organic Semiconductors. *Nature* **2005**, *434*, 194–199.
- (8) Tang, C. W. 2-Layer Organic Photovoltaic Cell. *Appl. Phys. Lett.* **1986**, *48*, 183–185.
- (9) Nalwa, H.; Shirk, J. *Phthalocyanines: Properties and Applications*; VCH: New York, 1996; Vol. 4.
- (10) Shtein, M.; Mapel, J.; Benziger, J. B.; Forrest, S. R. Effects of Film Morphology and Gate Dielectric Surface Preparation on the Electrical Characteristics of Organic-Vapor-Phase-Deposited Pentacene Thin-Film Transistors. *Appl. Phys. Lett.* **2002**, *81*, 268–270.
- (11) Brédas, J. L.; Calbert, J. P.; da Silva Filho, D. A.; Cornil, J. Organic Semiconductors: A Theoretical Characterization of the Basic Parameters Governing Charge Transport. *Proc. Natl. Acad. Sci. U.S.A.* **2002**, *99*, 5804–5809.
- (12) Brédas, J. L.; Beljonne, D.; Coropceanu, V.; Cornil, J. Charge-Transfer and Energy-Transfer Processes in  $\pi$ -Conjugated Oligomers and Polymers: A Molecular Picture. *Chem. Rev.* **2004**, *104*, 4971–5003.
- (13) Romaner, L.; Heimel, G.; Brédas, J.-L.; Gerlach, A.; Schreiber, F.; Johnson, R. L.; Zegenhagen, J.; Duhm, S.; Koch, N.; Zojer, E. Impact of Bidirectional Charge Transfer and Molecular Distortions on the Electronic Structure of a Metal-Organic Interface. *Phys. Rev. Lett.* **2007**, *99*, 256801–1–4.
- (14) Rangger, G. M.; Hofmann, O. T.; Romaner, L.; Heimel, G.; Bröker, B.; Blum, R. P.; Johnson, R. L.; Koch, N.; Zojer, E. F4TCNQ on Cu, Ag, and Au as prototypical example for a strong organic acceptor on coinage metals. *Phys. Rev. B* **2009**, *79*, 165306–1–12.
- (15) Tseng, T. C.; Urban, C.; Wang, Y.; Otero, R.; Tait, S. L.; Alcami, M.; Ććija, D.; Trelka, M.; Gallego, J. M.; Lin, N.; et al. Charge-Transfer-Induced Structural Rearrangements at Both Sides of Organic/Metal Interfaces. *Nat. Chem.* **2010**, *2*, 374–379.
- (16) Heimel, G.; Duhm, S.; Salzmann, I.; Gerlach, A.; Strozecka, A.; Niederhausen, J.; Bürker, C.; Hosokai, T.; Fernandez-Torrente, I.; Schulze, G.; et al. Charged and Metallic Molecular Monolayers through Surface-Induced Aromatic Stabilization. *Nat. Chem.* **2013**, *5*, 187–194.
- (17) Bröker, B.; Hofmann, O. T.; Rangger, G. M.; Frank, P.; Blum, R. P.; Rieger, R.; Venema, L.; Vollmer, A.; Müllen, K.; Rabe, J. P.; et al. Density-Dependent Reorientation and Rehybridization of Chemisorbed Conjugated Molecules for Controlling Interface Electronic Structure. *Phys. Rev. Lett.* **2010**, *104*, 246805–1–4.
- (18) Glöckler, K.; Seidel, C.; Soukopp, A.; Sokolowski, M.; Umbach, E.; Böhringer, M.; Berndt, R.; Schneider, W. D. Highly Ordered Structures and Submolecular Scanning Tunneling Microscopy Contrast of PTCDA and DM-PBDCI Monolayers on Ag(111) and Ag(110). *Surf. Sci.* **1998**, *405*, 1–20.
- (19) Schmitz-Hübsch, T.; Fritz, T.; Staub, R.; Back, A.; Armstrong, N. R.; Leo, K. Structure of 3,4,9,10-Perylene-Tetracarboxylic-Dianhydride Grown on Reconstructed and Unreconstructed Au(100). *Surf. Sci.* **1999**, *437*, 163–172.
- (20) Tautz, F. S.; Sloboshanin, S.; Shklover, V.; Scholz, R.; Sokolowski, M.; Schaefer, J. A.; Umbach, E. Substrate Influence on the Ordering of Organic Submonolayers: A Comparative Study of PTCDA on Ag(110) and Ag(111) Using HREELS. *Appl. Surf. Sci.* **2000**, *166*, 363–369.
- (21) Oehzelt, M.; Grill, L.; Berkebile, S.; Koller, G.; Netzer, F. P.; Ramsey, M. G. The Molecular Orientation of Para-Sexiphenyl on Cu(110) and Cu(110) p(2 × 1)O. *ChemPhysChem* **2007**, *8*, 1707–1712.
- (22) Oehzelt, M.; Berkebile, S.; Koller, G.; Ivanco, J.; Surnev, S.; Ramsey, M. G.  $\alpha$ -Sexithiophene on Cu(110) and Cu(110)-(2 × 1)O: An STM and NEXAFS Study. *Surf. Sci.* **2009**, *603*, 412–418.
- (23) Sun, L. D.; Gall, J.; Weidinger, G.; Liu, C. Y.; Denk, M.; Zeppenfeld, P. Azimuthal Reorientation of Pentacene upon 2D Condensation. *Phys. Rev. Lett.* **2013**, *110*, 106101–1–5.
- (24) Ruffieux, P.; Gröning, O.; Biemann, M.; Simpson, C.; Müllen, K.; Schlapbach, L.; Gröning, P. Supramolecular Columns of Hexabenzocoronenes on Copper and Gold (111) surfaces. *Phys. Rev. B* **2002**, *66*, 073409–1–4.
- (25) Koller, G.; Berkebile, S.; Krenn, J. R.; Tzvetkov, G.; Hlawacek, G.; Lengyel, O.; Netzer, F. P.; Teichert, C.; Resel, R.; Ramsey, M. G. Oriented Sexiphenyl Single Crystal Nanoneedles on TiO<sub>2</sub> (110). *Adv. Mater.* **2004**, *16*, 2159–2162.
- (26) Koini, M.; Haber, T.; Werzer, O.; Berkebile, S.; Koller, G.; Oehzelt, M.; Ramsey, M. G.; Resel, R. Epitaxial Order of Pentacene on Cu(110)-(2 × 1)O: One Dimensional Alignment Induced by Surface Corrugation. *Thin Solid Films* **2008**, *517*, 483–487.
- (27) Klappenberger, F.; Kühne, D.; Marschall, M.; Neppel, S.; Krenner, W.; Nefedov, A.; Strunskus, T.; Fink, K.; Wööl, C.; Klyatskaya, S.; et al. Uniform  $\pi$ -System Alignment in Thin Films of Template-Grown Dicarboxylic-Oligophenyls. *Adv. Funct. Mater.* **2011**, *21*, 1631–1642.
- (28) Gundlach, D. J.; Lin, Y. Y.; Jackson, T. N.; Schlom, D. G. Oligophenyl-Based Organic Thin Film Transistors. *Appl. Phys. Lett.* **1997**, *71*, 3853–3855.
- (29) Resel, R. Crystallographic Studies on Hexaphenyl Thin Films - a Review. *Thin Solid Films* **2003**, *433*, 1–11.

- (30) Tasch, S.; Brandstätter, C.; Meghdadi, F.; Leising, G.; Froyer, G.; Athouel, L. Red-Green-Blue Light Emission From a Thin Film Electroluminescence Device Based on Parahexaphenyl. *Adv. Mater.* **1997**, *9*, 33–36.
- (31) Era, M.; Tsutsui, T.; Saito, S. Polarized Electroluminescence from Oriented p-Sexiphenyl Vacuum-Deposited Film. *Appl. Phys. Lett.* **1995**, *67*, 2436–2438.
- (32) Baudour, J. L.; Cailleau, H.; Yelon, W. B. Structural Phase-Transition in Polyphenyls. IV. Double-Well Potential in Disordered Phase of p-Terphenyl from Neutron (200 K) and X-Ray (Room-Temperature) Diffraction Data. *Acta Crystallogr. Sect. B-Struct. Commun.* **1977**, *33*, 1773–1780.
- (33) Baudour, J.-L.; Delugeard, Y.; Rivet, P. Structural Phase-Transition in Polyphenyls. VI. Crystal-Structure of Low-Temperature Ordered Phase of Para-Quaterphenyl at 110 K. *Acta Crystallogr. Sect. B-Struct. Commun.* **1978**, *34*, 625–628.
- (34) Müllegger, S.; Hänel, K.; Strunskus, T.; Wöll, C.; Winkler, A. Organic Molecular Beam Deposition of Oligophenyls on Au(111): A Study by X-Ray Absorption Spectroscopy. *ChemPhysChem* **2006**, *7*, 2552–2558.
- (35) Müllegger, S.; Winkler, A. Hexaphenyl Thin Films on Clean and Carbon Covered Au(111) Studied with TDS and LEED. *Surf. Sci.* **2006**, *600*, 1290–1299.
- (36) Schlickum, U.; Decker, R.; Klappenberger, F.; Zoppellaro, G.; Klyatskaya, S.; Auwärter, W.; Neppel, S.; Kern, K.; Brune, H.; Ruben, M.; et al. Chiral Kagomé Lattice from Simple Ditopic Molecular Bricks. *J. Am. Chem. Soc.* **2008**, *130*, 11776–11782.
- (37) Marschall, M.; Reichert, J.; Seufert, K.; Auwärter, W.; Klappenberger, F.; Weber-Bargioni, A.; Klyatskaya, S.; Zoppellaro, G.; Nefedov, A.; Strunskus, T.; et al. Supramolecular Organization and Chiral Resolution of p-Terphenyl-m-Dicarbonitrile on the Ag(111) Surface. *ChemPhysChem* **2010**, *11*, 1446–1451.
- (38) Kühne, D.; Klappenberger, F.; Decker, R.; Schlickum, U.; Brune, H.; Klyatskaya, S.; Ruben, M.; Barth, J. V. Self-Assembly of Nanoporous Chiral Networks with Varying Symmetry from Sexiphenyl-Dicarbonitrile on Ag(111). *J. Phys. Chem. C* **2009**, *113*, 17851–17859.
- (39) Schlickum, U.; Decker, R.; Klappenberger, F.; Zoppellaro, G.; Klyatskaya, S.; Ruben, M.; Silanes, I.; Arnau, A.; Kern, K.; Brune, H.; et al. Metal-Organic Honeycomb Nanomeshes with Tunable Cavity Size. *Nano Lett.* **2007**, *7*, 3813–3817.
- (40) Decker, R.; Schlickum, U.; Klappenberger, F.; Zoppellaro, G.; Klyatskaya, S.; Ruben, M.; Barth, J. V.; Brune, H. Using metal-organic templates to steer the growth of Fe and Co nanocluster. *Appl. Phys. Lett.* **2008**, *93*, 243102–1–3.
- (41) Kühne, D.; Klappenberger, F.; Decker, R.; Schlickum, U.; Brune, H.; Klyatskaya, S.; Ruben, M.; Barth, J. V. High-Quality 2D Metal-Organic Coordination Network Providing Giant Cavities within Mesoscale Domains. *J. Am. Chem. Soc.* **2009**, *131*, 3881–3883.
- (42) Kühne, D.; Klappenberger, F.; Krenner, W.; Klyatskaya, S.; Ruben, M.; Barth, J. V. Rotational and constitutional dynamics of caged supramolecules. *Proc. Natl. Acad. Sci. U.S.A.* **2010**, *107*, 21332–21336.
- (43) Schlickum, U.; Klappenberger, F.; Decker, R.; Zoppellaro, G.; Klyatskaya, S.; Ruben, M.; Kern, K.; Brune, H.; Barth, J. V. Surface-Confined Metal-Organic Nanostructures from Co-Directed Assembly of Linear Terphenyl-dicarbonitrile Linkers on Ag(111). *J. Phys. Chem. C* **2010**, *114*, 15602–15606.
- (44) Marschall, M.; Reichert, J.; Weber-Bargioni, A.; Seufert, K.; Auwärter, W.; Klyatskaya, S.; Zoppellaro, G.; Ruben, M.; Barth, J. V. Random Two-Dimensional String Networks Based on Divergent Coordination Assembly. *Nat. Chem.* **2010**, *2*, 131–137.
- (45) Klappenberger, F.; Kühne, D.; Krenner, W.; Silanes, I.; Arnau, A.; Garcia de Abajo, F. J.; Klyatskaya, S.; Ruben, M.; Barth, J. V. Tunable Quantum Dot Arrays Formed from Self-Assembled Metal-Organic Networks. *Phys. Rev. Lett.* **2011**, *106*, 026802–1–4.
- (46) Klyatskaya, S.; Klappenberger, F.; Schlickum, U.; Kühne, D.; Marschall, M.; Reichert, J.; Decker, R.; Krenner, W.; Zoppellaro, G.; Brune, H.; et al. Surface-Confined Self-Assembly of Di-Carbonitrile Polyphenyls. *Adv. Funct. Mater.* **2011**, *21*, 1230–1240.
- (47) Klappenberger, F. Two-dimensional Functional Molecular Nanoarchitectures - Complementary Investigations with Scanning Tunneling Microscopy and X-ray Spectroscopy. *Prog. Surf. Sci.* **2014**, *89*, 1–55.
- (48) Arras, E.; Seitsonen, A. P.; Klappenberger, F.; Barth, J. V. Nature of the Attractive Interaction Between Proton Acceptors and Organic Ring Systems. *Phys. Chem. Chem. Phys.* **2012**, *14*, 15995–16001.
- (49) Cañas-Ventura, M. E.; Klappenberger, F.; Clair, S.; Pons, S.; Kern, K.; Brune, H.; Strunskus, T.; Wöll, C.; Fasel, R.; Barth, J. V. Coexistence of One- and Two-Dimensional Supramolecular Assemblies of Terephthalic Acid on Pd(111) due to Self-Limiting Deprotonation. *J. Chem. Phys.* **2006**, *125*, 184710–1–8.
- (50) Kresse, G.; Furthmüller, J. Efficiency of Ab-Initio Total Energy Calculations for Metals and Semiconductors Using a Plane-Wave Basis Set. *Comput. Mater. Sci.* **1996**, *6*, 15–50.
- (51) Kresse, G.; Furthmüller, J. Efficient Iterative Schemes for Ab Initio Total-Energy Calculations Using a Plane-Wave Basis Set. *Phys. Rev. B* **1996**, *54*, 11169–11186.
- (52) Perdew, J. P.; Burke, K.; Ernzerhof, M. Generalized gradient approximation made simple. *Phys. Rev. Lett.* **1996**, *77*, 3865–3868.
- (53) Grimme, S. Semiempirical GGA-type density functional constructed with a long-range dispersion correction. *J. Comput. Chem.* **2006**, *27*, 1787–1799.
- (54) Blöchl, P. E. Projector Augmented-Wave Method. *Phys. Rev. B* **1994**, *50*, 17953–17979.
- (55) Kresse, G.; Joubert, D. From ultrasoft pseudopotentials to the projector augmented wave method. *Phys. Rev. B* **1999**, *59*, 1758–1775.
- (56) Monkhorst, H. J.; Pack, J. D. Special Points for Brillouin-Zone Integrations. *Phys. Rev. B* **1976**, *13*, 5188–5192.
- (57) Bordat, P.; Brown, R. A Molecular Model of p-Terphenyl and its Disorder-Order Transition. *Chem. Phys.* **1999**, *246*, 323–334.
- (58) Yokoyama, T.; Yokoyama, S.; Kamikado, T.; Okuno, Y.; Mashiko, S. Selective Assembly on a Surface of Supramolecular Aggregates with Controlled Size and Shape. *Nature* **2001**, *413*, 619–621.
- (59) Henningsen, N.; Rurali, R.; Limbach, C.; Drost, R.; Pascual, J. I.; Franke, K. J. Site-Dependent Coordination Bonding in Self-Assembled Metal-Organic Networks. *J. Phys. Chem. Lett.* **2011**, *2*, 55–61.
- (60) Makoudi, Y.; Arras, E.; Kepčija, N.; Krenner, W.; Klyatskaya, S.; Klappenberger, F.; Ruben, M.; Seitsonen, A. P.; Barth, J. V. Hierarchically Organized Bimolecular Ladder Network Exhibiting Guided One-Dimensional Diffusion. *ACS Nano* **2012**, *6*, 549–556.
- (61) Krenner, W.; Klappenberger, F.; Kepčija, N.; Arras, E.; Makoudi, Y.; Kühne, D.; Klyatskaya, S.; Ruben, M.; Barth, J. V. Unraveling the Hierarchical Formation of Open-porous Bimolecular Networks. *J. Phys. Chem. C* **2012**, *116*, 16421–16429.
- (62) Okuno, Y.; Yokoyama, T.; Yokoyama, S.; Kamikado, T.; Mashiko, S. Theoretical Study of Benzonitrile Clusters in the Gas Phase and their Adsorption onto a Au(111) surface. *J. Am. Chem. Soc.* **2002**, *124*, 7218–7225.
- (63) Barth, J. V. Fresh Perspectives for Surface Coordination Chemistry. *Surf. Sci.* **2009**, *603*, 1533–1541.
- (64) Pawin, G.; Wong, K. L.; Kim, D.; Sun, D. Z.; Bartels, L.; Hong, S.; Rahman, T. S.; Carp, R.; Marsella, M. A Surface Coordination Network Based on Substrate-Derived Metal Adatoms with Local Charge Excess. *Angew. Chem., Int. Ed.* **2008**, *47*, 8442–8445.
- (65) Kwon, K. Y.; Lin, X.; Pawin, G.; Wong, K.; Bartels, L. Oxadiazole-Metal Interface: from Isolated Molecules to  $\pi$ -Stacking. *Langmuir* **2006**, *22*, 857–859.
- (66) Dufflot, D.; Flament, J. P.; Heinesch, J.; Hubin-Franskin, M. J. Re-analysis of the K-Shell Spectrum of Benzene. *J. Electron Spectrosc. Relat. Phenom.* **2000**, *113*, 79–90.
- (67) Püttner, R.; Kolczewski, C.; Martins, M.; Schlachter, A. S.; Snell, G.; Sant'Anna, M.; Viehhaus, J.; Hermann, K.; Kaindl, G. The C 1s NEXAFS Spectrum of Benzene Below Threshold: Rydberg or Valence

Character of the Unoccupied  $\sigma$ -Type Orbitals. *Chem. Phys. Lett.* **2004**, *393*, 361–366.

(68) Reiss, S.; Krumm, H.; Niklewski, A.; Staemmler, V.; Wöll, C. The Adsorption of Acenes on Rutile TiO<sub>2</sub>(110): A Multi-Technique Investigation. *J. Chem. Phys.* **2002**, *116*, 7704–7713.

(69) Rangan, S.; Gallet, J. J.; Bourmel, F.; Kubsky, S.; Le Guen, K.; Dufour, G.; Rochet, F.; Sirotti, F.; Carniato, S.; Ilakovac, V. Adsorption of Benzonitrile on Si(001)-2 × 1 at 300 K. *Phys. Rev. B* **2005**, *71*, 165318–1–12.

(70) Piantek, M.; Miguel, J.; Krüger, A.; Navío, C.; Bernien, M.; Ball, D. K.; Hermann, K.; Kuch, W. Temperature, Surface, and Coverage-Induced Conformational Changes of Azobenzene Derivatives on Cu(001). *J. Phys. Chem. C* **2009**, *113*, 20307–20315.

(71) Rennie, E. E.; Kempgens, B.; Köppe, H. M.; Hergenbahn, U.; Feldhaus, J.; Itchkawitz, B. S.; Kilcoyne, A. L. D.; Kivimäki, A.; Maier, K.; Piancastelli, M. N.; et al. A comprehensive Photoabsorption, Photoionization, and Shake-Up Excitation Study of the C 1s Cross Section of Benzene. *J. Chem. Phys.* **2000**, *113*, 7362–7375.

(72) Stöhr, J. *NEXAFS Spectroscopy*; Springer-Verlag: Berlin, 1992.

(73) Carniato, S.; Ilakovac, V.; Gallet, J. J.; Kukk, E.; Luo, Y. Hybrid density-Functional Theory Calculations of Near-Edge X-Ray Absorption Fine-Structure Spectra: Applications on Benzonitrile in Gas Phase. *Phys. Rev. A* **2005**, *71*, 022511–1–11.

(74) Karimi, M.; Tomkowsky, T.; Vidali, G.; Biham, O. Diffusion of Cu on Cu surfaces. *Phys. Rev. B* **1995**, *52*, 5364–5374.

(75) Perry, C. C.; Haq, S.; Frederick, B. G.; Richardson, N. V. Face Specificity and the Role of Metal Adatoms in Molecular Reorientation at Surfaces. *Surf. Sci.* **1998**, *409*, 512–520.

(76) Tseng, T. C.; Lin, C. S.; Shi, X. Q.; Tait, S. L.; Liu, X.; Starke, U.; Lin, N.; Zhang, R. Q.; Minot, C.; Van Hove, M. A.; et al. Two-dimensional metal-organic coordination networks of Mn-7,7,8,8-tetracyanoquinodimethane assembled on Cu(100): Structural, electronic, and magnetic properties. *Phys. Rev. B* **2009**, *80*, 155458–1–6.

(77) Klappenberger, F.; Weber-Bargioni, A.; Auwärter, W.; Marschall, M.; Schiffrin, A.; Barth, J. V. Temperature Dependence of Conformation, Chemical State and Metal-Directed Assembly of Tetrapyrrolyl-Porphyrin on Cu(111). *J. Chem. Phys.* **2008**, *129*, 214702–1–10.

(78) Heim, D.; Ćecija, D.; Seufert, K.; Auwärter, W.; Aurisicchio, C.; Fabbro, C.; Bonifazi, D.; Barth, J. V. Self-Assembly of Flexible One-Dimensional Coordination Polymers on Metal Surfaces. *J. Am. Chem. Soc.* **2010**, *132*, 6783–6790.

(79) Heim, D.; Seufert, K.; Auwärter, W.; Aurisicchio, C.; Fabbro, C.; Bonifazi, D.; Barth, J. V. Surface-Assisted Assembly of Discrete Porphyrin-Based Cyclic Supramolecules. *Nano Lett.* **2010**, *10*, 122–128.

(80) Matena, M.; Stöhr, M.; Riehm, T.; Björk, J.; Martens, S.; Dyer, M. S.; Persson, M.; Lobo-Checa, J.; Müller, K.; Enache, M.; et al. Aggregation and Contingent Metal/Surface Reactivity of 1,3,8,10-Tetraazaperopyrene (TAPP) on Cu(111). *Chem.—Eur. J.* **2010**, *16*, 2079–2091.

(81) Walch, H.; Dienstmaier, J.; Eder, G.; Gutzler, R.; Schlogl, S.; Sirtl, T.; Das, K.; Schmittel, M.; Lackinger, M. Extended Two-Dimensional Metal-Organic Frameworks Based on Thiolate-Copper Coordination Bonds. *J. Am. Chem. Soc.* **2011**, *133*, 7909–7915.

(82) Ćecija, D.; Vijayaraghavan, S.; Auwärter, W.; Joshi, S.; Seufert, K.; Aurisicchio, C.; Bonifazi, D.; Barth, J. V. Two-Dimensional Short-Range Disordered Crystalline Networks from Flexible Molecular Modules. *ACS Nano* **2012**, *6*, 4258–4265.

(83) Sherrill, C. D.; Sumpter, B. G.; Sinnokrot, M. O.; Marshall, M. S.; Hohenstein, E. G.; Walker, R. C.; Gould, I. R. Assessment of Standard Force Field Models Against High-Quality Ab Initio Potential Curves for Prototypes of  $\pi$ - $\pi$ , CH/ $\pi$ , and SH/ $\pi$  Interactions. *J. Comput. Chem.* **2009**, *30*, 2187–2193.